Electric Power Systems Research 229 (2024) 110186

Contents lists available at ScienceDirect

Electric Power Systems Research

journal homepage: www.elsevier.com/locate/epsr

A communication-saving distributed secondary control of hybrid AC/DC microgrids and its small-signal analysis

Chang Yang, Tao Zheng *, Ming Bu, Pengyu Li

The Shaanxi Key Laboratory of Smart Grid, School of Electrical Engineering, Xi'an JiaoTong University, Xi'an, 710049, Shannxi, China

ARTICLE INFO

Keywords:
Communication-saving
Distributed secondary control (DSC)
Hybrid AC/DC microgrid
Small-signal analysis

ABSTRACT

Distributed secondary control (DSC) is an efficient way to realize power sharing among distributed generators (DGs) and restore the voltage deviation caused by droop control. Traditional DSC strategy of a hybrid AC/DC microgrid (MG) needs multiple communication links between interlinking converter (IC) and DGs, which makes the communication network complex and affects DG's plug&play capability. In this paper, a communication-saving DSC strategy of hybrid AC/DC MG is proposed. Local communications in both ac-MG and dc-MG plus an intercommunication between them are designed for power reference adjustment. Accurate power sharing among all of the DGs can be realized without communicating with IC. A small-signal model of the hybrid system is established for stability analysis and the range of control parameters can be adjusted based on this model. Experiments are carried out to demonstrate the proposed DSC strategy under different operating conditions.

1. Introduction

Nowadays, MG attracts much attention because it not only provides an energy interface to DGs but also improves the reliability of power supply under extreme conditions [1]. Most DGs output DC power and extra equipment is required when accessing an AC grid, which undoubtedly reduces the conversion efficiency [2]. Emergence of AC/DC MG provides a way to handle this problem. Its hybrid structure involves several ac-MGs and dc-MGs interconnected through the IC, which controls the power exchange of both sides. The challenge in such a hybrid grid is to design the control strategy, especially power sharing among all the DGs with coordination of the IC.

In general, MG control can be performed in three layers: primary control layer, secondary control (SC) layer and tertiary control layer [3,4]. Primary control determines a single DG's output characteristic, e.g. droop control. Secondary control manages power sharing and voltage restoration throughout the MG. Tertiary control is responsible for optimal control and economic operation [5,6]. To implement SC, centralized control, decentralized control and distributed control are adopted [7]. Different SC strategies are summarized in Table 1. Various SC strategies have been used to realize frequency restoration [1,8], voltage restoration [1,8,9], power sharing [10–12], unbalanced load compensation [13] in a single ac-MG and DC voltage restoration [14–17], power sharing [15,18,19] in a single dc-MG.

In an AC/DC MG, SC is expected to control the normal operation of each MG and to manage the power sharing with the assistance of IC. Several centralized SC strategies have been adopted in AC/DC MGs [4,20–22], where a central controller is used to collect global information and issue power instructions to the IC and DGs. In [4], a centralized SC and tertiary control are used to manage power sharing on both sides of the hybrid MG and accurate power sharing can be achieved on each side. In [20], coordination control is proposed to realize power support between ac-MG and dc-MG. Instead of droop control, maximum power point tracking (MPPT) is adopted to make full use of energy utilization. In [21], constant DC voltage control of IC is employed to restore the DC voltage and realize the power support in different MGs simultaneously. In [22], a state-machine-based central controller is designed and the IC is able to switch operation mode following the change of loads. However, in the above-mentioned control strategies, communication between the central controller and each DG is required. Controller or communication failure will render the power sharing to be difficult and even lead to an unstable operation. In addition to the centralized SC strategy, decentralized SC strategies have been intensively investigated [23–26], where communication is not required but complicated controller design is inevitable. Due to the lack of information exchange among DGs, power sharing may deviate from expectations. In [23], a decentralized power control and management strategy of the AC/DC MG is proposed, but the bus voltage of ac-MG is only supported by the IC during island mode and the voltage may collapse if the IC fails. A dual-droop control [24] and

* Corresponding author.
E-mail addresses: yangchang1996@stu.xjtu.edu.cn (C. Yang), tzheng@mail.xjtu.edu.cn (T. Zheng), bm1234@stu.xjtu.edu.cn (M. Bu), lipengyu0628@stu.xjtu.edu.cn (P. Li).

https://doi.org/10.1016/j.epsr.2024.110186
Received 29 May 2023; Received in revised form 3 January 2024; Accepted 22 January 2024

Table 1
Comparisons among different secondary control strategies.

Control mode	Microgrids	Advantages	Disadvantages	Literature
Centralized Control	AC DC AC/DC	1. easy implementation 2. information security	1. single point failure 2. communication required	[10,11,13] [14,18] [4,20–22]
Decentralized Control	AC DC AC/DC	1. free of communication; 2. plug&play capability	1. complex controller design 2. parameter dependence	[9,12] [15,27] [23–26]
Distributed Control	AC DC AC/DC	1. strong robustness 2. plug&play capability	1. communication required 2. vulnerable to cyber attack	[1,8,28–30] [16,17,19,31] [32–36]

a $P_{dc} - U_{dc}^2$ droop control [25,26] for the IC are proposed based on decentralized control. However, proportional power dispatch in the hybrid MG is hard to be realized since the coordination power control between ac-DG and dc-DG is ignored.

Recently, the distributed control strategy has received much attention. Local information is exchanged between the neighbor DGs through a communication system and power sharing among DGs can be achieved. Distributed control strategy mitigates the effect of single-point failure and improves the robustness of the control system. The challenge is to design the control strategy of IC and build an efficient communication network. In [32,33], a distributed consistency algorithm is proposed to coordinate the local information obtained from ac-DG and dc-DG in order to dynamically adjust the power reference of the IC. Due to the inevitable communication linking IC and DGs, the communication load of IC increases greatly as multiple DGs access the MG. In this case, voltage and frequency deviation may occur if the IC communication fails. In [34], a distributed coordination control strategy of AC/DC MG is proposed, and the DSC serves in the ac-MG and dc-MG independently. Therefore, it is difficult to fulfill a global power sharing between both MGs. In [35], a distributed uniform control of parallel ICs is proposed and accurate power sharing in different ICs is realized, where power coordination in the whole MG is not taken into account. In [36], optimal power sharing among all the DGs can be achieved by combining the DSC with a decentralized primary control. Both the frequency of the ac-MG and the weighted average DC voltage can be precisely restored to their rated values. However, a complex communication is required to achieve the optimal control performance. In addition, the above mentioned strategies have not addressed the reactive power support capability of the IC. In practice, IC usually does not operate at its full load since its rated capacity is designed greater than the maximum unbalanced load of ac-MG and dc-MG [37]. The spare capacity can be utilized to support the reactive power of the ac-MG.

To release the heavy burden of data exchange and improve control flexibility, this paper presents a novel DSC strategy applied for AC/DC MGs. The main contributions are expected in the following.

1. A communication-saving control strategy is proposed for achieving power sharing among DGs in the hybrid AC/DC MG. Without IC communication, the proposed DSC can mitigate issues associated with IC communication failures and simplify the communication network. The IC can function as a transfer station, adjusting its output power using the local information.
2. A small-signal model of the AC/DC MG, incorporating the proposed DSC, is formulated using transfer function matrix. Small-signal stability analysis facilitates the assessment of control performance under different control parameters and communication delays.
3. A laboratory AC/DC MG is developed with actual power converters, allowing for the validation of the proposed control strategy under different operating conditions. Comparative analyses are performed to evaluate the distinctions between the DSC with and without IC communication.

The rest of this paper is organized as follows. The DSC of an AC/DC MG is presented in Section 2. A small-signal model of the AC/DC MG is established and small-signal stability analysis is conducted in Section 3. Experiments are carried out to show the performance of the proposed control strategy under various operating conditions in Section 4. Finally, Some discussions and conclusions are given in Section 5 and Section 6 respectively.

2. Secondary control strategy in AC/DC MG

In order to achieve power sharing in a MG, DSC strategy uses neighbor information of DGs. Thus, fewer communication links are required and the control becomes more reliable. In a hybrid MG, the traditional DSC strategy requires IC to communicate with DGs in both ac-MG and dc-MG for power balance control. With more DGs integrated, communications become complicated. In this paper, IC is left alone and communication links only exist among the DGs of the MGs.

For notional convenience in the following sections, DGs that are integrated in ac-MG are indexed from 1 to $\mathcal{N}_{ac}$ while DGs in dc-MG are indexed from $\mathcal{N}_{ac}+1$ to $\mathcal{N}_{ac}+\mathcal{N}_{dc}$, where $\mathcal{N}_{ac}$ and $\mathcal{N}_{dc}$ indicate the total number of DGs in ac-MG and dc-MG respectively.

2.1. Framework of the control strategy

In DSC, communication performance will affect the dynamic characteristics of the control system and communication network design is significant. As shown in Fig. 1(a), the communication system in this paper is composed of three subsystems: two local communication networks (dotted lines) in ac-MG and dc-MG respectively, and intercommunication links between ac-MG and dc-MG (dashed lines). Local communication enables power sharing within either subgrid. For instance, in the ac-MG, local communication allows ac-DGs to exchange active/reactive power information and share the output power. In the dc-MG, local communication manages active power information exchange and power sharing among dc-DGs. Intercommunication is primarily responsible for achieving active power balance across both subgrids. In the proposed control strategy, local communication is indispensable, while intercommunication may be omitted. Without intercommunication, a distributed communication network can only achieve power sharing within a single subgrid. Power distribution between the ac-DGs and dc-DGs depends on loading conditions in different subgrids, which makes it difficult to share power among them.

In Fig. 1(a), all communication links can be represented as an undirected graph $G = (\mathbb{V}, \mathbb{E}, A)$, where $\mathbb{V} = 1, 2, \ldots, \mathcal{N}_{ac}+\mathcal{N}_{dc}$ is a set of vertices, $\mathbb{E} \subset \mathbb{V} \times \mathbb{V}$ is a set of edges and A is the adjacency matrix. The entry of the adjacency matrix is defined as (1). In order to ensure the participation of all DGs in the distributed secondary control, the undirected graph of all the vertices must be fully connected. Otherwise, the DG which is not interconnected will be unable to share power with others.

$$a_{ij} = \begin{cases} 1 & \text{if } (i,j) \in \mathbb{E} \\ 0 & \text{otherwise} \end{cases} \tag{1}$$

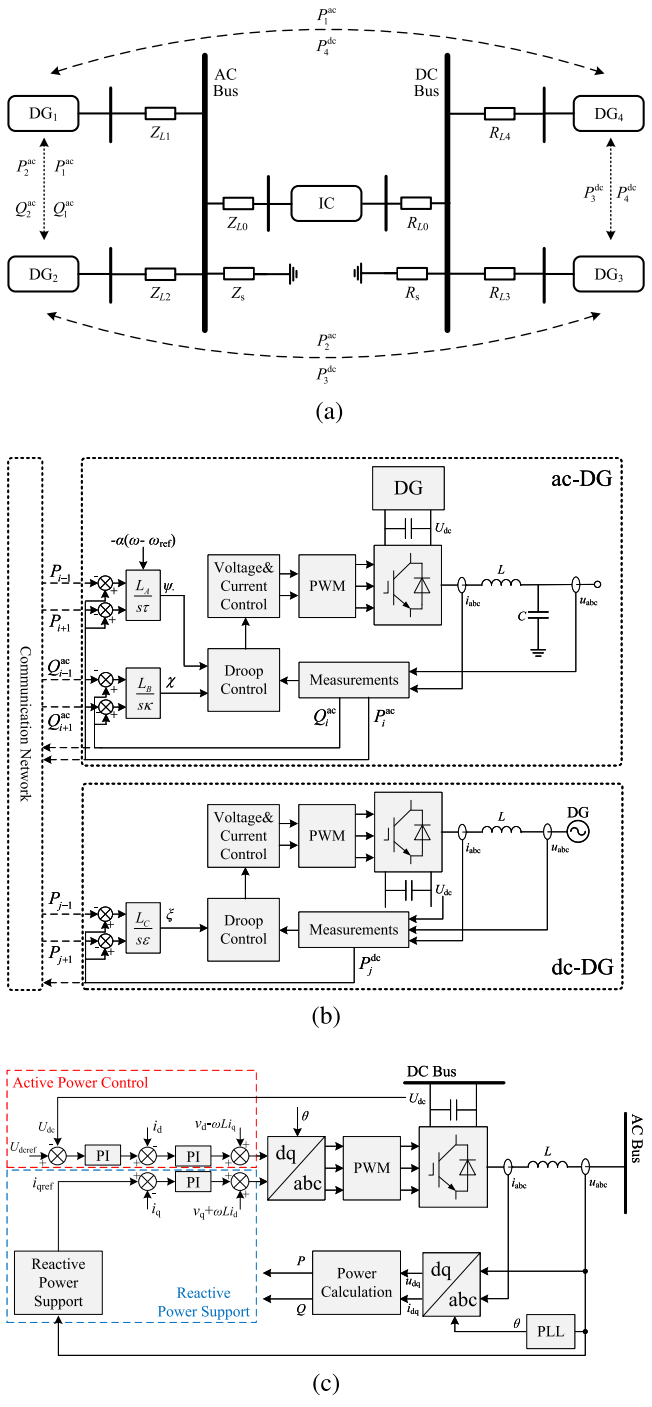

Fig. 1. Framework of the proposed control strategy. (a) communication links, (b) block diagram of ac-DG and dc-DG control, (c) block diagram of IC control.

2.2. DSC strategy of ac-DG and dc-DG

In an AC/DC MG, SC provides two control functions: i. active power sharing through the whole hybrid MG and reactive power sharing in the ac-MG, regarding the rated capacity of DGs, ii. restoration of frequency to its rated values. In this paper, the droop control based DSC is depicted through (2)–(4), where (2) and (3) represent the DSC of the ac-DG, (4) describes the DSC of the dc-DG.

$$\begin{cases} \omega_i = \omega_{\text{ref}} - n_{\text{p}}(P_i^* - P_{\text{refi}}^*) + \psi_i \\ \tau_i \dfrac{d\psi_i}{dt} = -\alpha_i(\omega_i - \omega_{\text{ref}}) - \displaystyle\sum_{k=1}^{\mathcal{N}_{\text{ac}}+\mathcal{N}_{\text{dc}}} a_{ik}(P_i^* - P_k^*) \\ i \in [1, 2, \ldots, \mathcal{N}_{\text{ac}}] \end{cases} \tag{2}$$

$$\begin{cases} u_i = U_{\text{ref}} - n_{\text{q}}(Q_i^* - Q_{\text{refi}}^*) + \chi_i \\ \kappa_i \dfrac{d\chi_i}{dt} = -\displaystyle\sum_{k=1}^{\mathcal{N}_{\text{ac}}} b_{ik}(Q_i^* - Q_k^*) \\ i \in [1, 2, \ldots, \mathcal{N}_{\text{ac}}] \end{cases} \tag{3}$$

$$\begin{cases} u_{\text{dc}j} = U_{\text{dcref}} - n_{\text{dc}}(P_j^* - P_{\text{dcref}j}^*) + \zeta_j \\ \epsilon_j \dfrac{d\zeta_j}{dt} = -\displaystyle\sum_{k=1}^{\mathcal{N}_{\text{ac}}+\mathcal{N}_{\text{dc}}} c_{jk}(P_j^* - P_k^*) \\ j \in [\mathcal{N}_{\text{ac}}+1, \mathcal{N}_{\text{ac}}+2, \ldots, \mathcal{N}_{\text{ac}}+\mathcal{N}_{\text{dc}}] \end{cases} \tag{4}$$

where ω_{ref}, U_{ref} and U_{dcref} are the reference of angular frequency, AC voltage and DC voltage, respectively. n_{p}, n_{q} and n_{dc} are the coefficients of $P_{\text{ac}} - f$, $Q_{\text{ac}} - U_{\text{ac}}$ and $P_{\text{dc}} - U_{\text{dc}}$ droop control. $P^* = P/S_{\text{rated}}$ and $Q^* = Q/S_{\text{rated}}$ are the unit output values of active power and reactive power where S_{rated} is the rated power. ω_i, u_i and $u_{\text{dc}j}$ are the angular frequency, AC voltage and DC voltage of DG_i (or DG_j). P_{ref}^* and Q_{ref}^* are the active and reactive power reference. α_i is the restoration factor of frequency, which restricts the frequency deviation. τ_i, κ_i and ϵ_j are the control parameters of DSC. a_{ik}, b_{ik} and c_{jk} are denoted as the entries of the communication adjacency matrices of different DSCs. ψ_i, χ_i, and ζ_j are compensation terms of the droop control.

The equations in (2)–(4) can effectively eliminate the impact of the line impedance on power sharing by introducing compensation terms ψ_i, χ_i and ζ_j. Taking Eq. (2) as an example, ψ_i is adjusted until the conditions $\omega_i = \omega_{\text{ref}}$ and $P_i^* = P_k^*$ are met. Similar analysis analyses can be applied to Eqs. (3) and (4). Therefore, achieving power sharing among DGs is feasible through a distributed control algorithm, where the power information from the adjacent DG is necessary to be obtained.

2.3. Control strategy of IC

Due to the unbalanced load between ac-MG and dc-MG, the IC is used to help manage active power sharing in the hybrid MG. If the load is heavier in ac-MG, IC will serve as a bridge to transfer active power from dc-MG to ac-MG and vice versa. Besides, the IC is also responsible for regulating the DC voltage and supporting the AC voltage. Herein, an IC control strategy is designed which is different from the traditional DSC that uses IC communication. The active control involved in this strategy is to perform power sharing and restrict the DC voltage deviation, while the reactive control involved is to support voltage in the ac-MG.

2.3.1. Active power control strategy

Using DSC, the IC is able to control the power sharing in a hybrid MG. However, power reference depends on the power information exchanged between ac-DG and dc-DG. In the proposed DSC, the IC adopts DC voltage control instead of power control for easy realization without IC communication. The active control strategy of the IC is described in Fig. 1(c). By setting a constant DC voltage value, IC maintains its DC voltage to this reference, which can be a benchmark for the dc-DGs in the dc-MG. Following (4), the dc-DGs adjust their DC voltages to change the power flow. The output power of the IC changes accordingly and the power balance between both MGs is achieved with the cooperation of IC and DGs. The proposed control strategy enables the IC to transfer active power from the dc-MG to the ac-MG in the presence of heavy loads on the ac-MG. Conversely, it allows power transfer from the ac-MG to the dc-MG when heavy loads are connected to the dc-MG. Herein, IC supports the DC voltage using local information, while power sharing is obtained through the control of DGs.

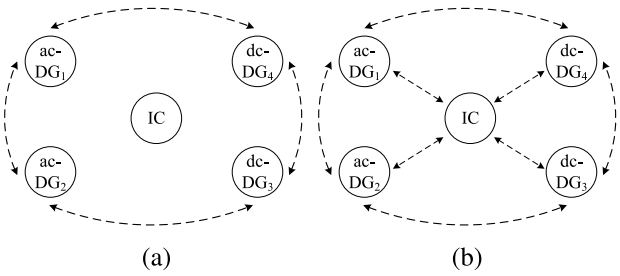

Fig. 2. Communication network of hybrid AC/DC MG. (a) without IC communication, (b) with IC communication.

2.3.2. Reactive power support

Generally, the rated power of IC is large enough to support active power streaming between ac-MG and dc-MG. Thus, the spare capacity can be utilized to support reactive power in ac-MG. Herein, a droop relation between the reactive power and the RMS value of AC voltage is employed for reactive power support, which can be expressed in (5).

$$i^{\mathrm{ic}}_{\mathrm{qref}} = n_{\mathrm{ic}}(V^{\mathrm{ic}}_{\mathrm{avg\_rms}} - V^{*}_{\mathrm{rms}}) \tag{5}$$

where $i^{\mathrm{ic}}_{\mathrm{qref}}$ is the reference of IC's reactive current. $i^{\mathrm{ic}}_{\mathrm{qref}} > 0$ indicates that IC absorbs reactive power from ac-MG. n_{ic} is the coefficient of the reactive power support control strategy. $V^{\mathrm{ic}}_{\mathrm{avg\_rms}} = (V^{\mathrm{ic}}_{\mathrm{a\_rms}} + V^{\mathrm{ic}}_{\mathrm{b\_rms}} + V^{\mathrm{ic}}_{\mathrm{c\_rms}})/3$ is the average value of AC voltage. V^{*}_{rms} is the rated AC voltage of IC.

2.4. Communication network

As discussed above, it is unnecessary to put IC into the communication system. The communication network involving IC or dismissing IC is illustrated in Fig. 2, which shows that a communication network for DSC can be divided into three subsystems: local communication within each sub-MG, intercommunication between different sub-MGs and IC communication. In these three subsystems, IC communication is significantly affected by the scale of the hybrid MG. The number of IC's communication links is equal to the number of DGs in the hybrid MG and the target number of possible links is $2(\mathcal{N}_{\mathrm{ac}}+\mathcal{N}_{\mathrm{dc}})$. However, if the IC does not communicate with the DGs, the number of communication links is $\mathcal{N}_{\mathrm{ac}}+\mathcal{N}_{\mathrm{dc}}$. Thus, a small number of communication links leads to less effect of communication failure on DSC.

3. Small-signal stability analysis

In this section, a small-signal model of the hybrid AC/DC MG considering the proposed control strategy is developed by using transfer function matrix. Thus the interplay between control parameters and the transient process of the DSC can be investigated, which facilitates the parameter design process.

3.1. Small-signal model

3.1.1. ac-DG and dc-DG model

Without loss of generality, the dynamic characteristic of the double loop control is ignored and DG uses droop control as the primary control [38]. For an ac-DG, the small-signal model of droop control can be expressed in (6) and (7).

$$\Delta\omega = \Delta\omega_{\mathrm{ref}} - n_{\mathrm{p}}(\Delta P_{\mathrm{ac}} - \Delta P_{\mathrm{acref}}) + \Delta\psi \tag{6}$$

$$\begin{cases} \Delta u_{\mathrm{d}} = \Delta U_{\mathrm{ref}} - n_{\mathrm{q}}(\Delta Q_{\mathrm{ac}} - \Delta Q_{\mathrm{acref}}) + \Delta\chi \\ \Delta u_{\mathrm{q}} = 0 \end{cases} \tag{7}$$

in the context of small-signal analysis, $\Delta\omega$ and $\Delta\omega_{\mathrm{ref}}$ are the angular frequency and its reference. ΔP_{ac} and $\Delta P_{\mathrm{acref}}$ are the active power and its reference. ΔQ_{ac} and $\Delta Q_{\mathrm{acref}}$ are the reactive power and its reference. Δu_{d} and Δu_{q} are the AC voltage in d-axis and q-axis respectively. ΔU_{ref} is the AC voltage reference. $\Delta\psi$ and $\Delta\chi$ are the DSC state variables.

As for a dc-DG, the small-signal model of droop control can be expressed in (8).

$$\Delta u_{\mathrm{dc}} = \Delta u_{\mathrm{dcref}} - n_{\mathrm{dc}}(\Delta P_{\mathrm{dc}} - \Delta P_{\mathrm{dcref}}) + \Delta\zeta \tag{8}$$

where Δu_{dc} and $\Delta u_{\mathrm{dcref}}$ are the DC voltage and its reference. ΔP_{dc} and $\Delta P_{\mathrm{dcref}}$ are the active power and its reference. $\Delta\zeta$ is the DSC state variable.

The small-signal model of DG's output power can be expressed in (9). The effect of u_{q} on the output power of an ac-DG is ignored since the reference of u_{q} is equal to 0.

$$\begin{cases} \Delta P_{\mathrm{ac}} = \dfrac{3}{2}\dfrac{\omega_{\mathrm{c}}}{s+\omega_{\mathrm{c}}}(U_{\mathrm{d}}\Delta i_{\mathrm{d}} + I_{\mathrm{d}}\Delta u_{\mathrm{d}}) \\ \Delta Q_{\mathrm{ac}} = \dfrac{3}{2}\dfrac{\omega_{\mathrm{c}}}{s+\omega_{\mathrm{c}}}(U_{\mathrm{d}}\Delta i_{\mathrm{q}} + I_{\mathrm{q}}\Delta u_{\mathrm{d}}) \\ \Delta P_{\mathrm{dc}} = \dfrac{\omega_{\mathrm{c}}}{s+\omega_{\mathrm{c}}}(U_{\mathrm{dc}}\Delta i_{\mathrm{dc}} + I_{\mathrm{dc}}\Delta u_{\mathrm{dc}}) \end{cases} \tag{9}$$

In (9), ω_{c} is the cutoff frequency of the power filter. U_{d} is the steady state AC voltage in the d-axis. I_{d} and I_{q} are the steady state value of AC current in the d-axis and q-axis respectively. U_{dc} is the steady state DC voltage and I_{dc} is the steady state DC current.

The small-signal model of DSC is expressed in (10). Since the coefficient α is not associated with communication variables [8], their effect on small-signal stability is not considered in this paper. Relevant discussion can be found in [8].

$$\begin{cases} s\tau_i\Delta\psi_i = -a_{(i-1)i}(\Delta P_i - \Delta P_{i-1}) - a_{i(i+1)}(\Delta P_i - \Delta P_{i+1}) \\ s\kappa_i\Delta\chi_i = -b_{(i-1)i}(\Delta Q_i - \Delta Q_{i-1}) - b_{i(i+1)}(\Delta Q_i - \Delta Q_{i+1}) \\ s\epsilon_j\Delta\zeta_j = -c_{(j-1)j}(\Delta P_j - \Delta P_{j-1}) - c_{j(j+1)}(\Delta P_j - \Delta P_{j+1}) \\ i \in [1,2,\ldots,\mathcal{N}_{\mathrm{ac}}] \quad j \in [\mathcal{N}_{\mathrm{ac}}+1, \mathcal{N}_{\mathrm{ac}}+2, \ldots, \mathcal{N}_{\mathrm{ac}}+\mathcal{N}_{\mathrm{dc}}] \end{cases} \tag{10}$$

Here, τ, κ and ϵ are the time constants of DSC.

3.1.2. IC model

The average value model is used to explore the small-signal of IC, which can be expressed by (11) and (12).

$$\begin{bmatrix} \Delta u_{\mathrm{d}} \\ \Delta u_{\mathrm{q}} \end{bmatrix} + \begin{bmatrix} R_{\mathrm{s}} + sL_{\mathrm{s}} & -\omega L_{\mathrm{s}} \\ \omega L_{\mathrm{s}} & sL_{\mathrm{s}} \end{bmatrix} \begin{bmatrix} \Delta i_{\mathrm{d}} \\ \Delta i_{\mathrm{q}} \end{bmatrix} = \frac{U_{\mathrm{dc}}}{2} \begin{bmatrix} \Delta d_{\mathrm{d}} \\ \Delta d_{\mathrm{q}} \end{bmatrix} + \frac{1}{2} \begin{bmatrix} D_{\mathrm{d}} \\ D_{\mathrm{q}} \end{bmatrix} \Delta u_{\mathrm{dc}} \tag{11}$$

$$sC_{\mathrm{dc}}\Delta u_{\mathrm{dc}} = \Delta i_{\mathrm{dc}} - \frac{3}{4}I_{\mathrm{d}}\Delta d_{\mathrm{d}} - \frac{3}{4}I_{\mathrm{q}}\Delta d_{\mathrm{q}} - \frac{3}{4}D_{\mathrm{d}}\Delta i_{\mathrm{d}} - \frac{3}{4}D_{\mathrm{q}}\Delta i_{\mathrm{q}} \tag{12}$$

where R_{s} and L_{s} are the resistance and inductance of the output filter of IC. ω is the angular frequency of the synchronous reference frame (SRF). Δd_{d} and Δd_{q} are the duty cycle in d-axis and q-axis respectively. D_{d} and D_{q} are the steady duty cycle.

The detailed small-signal model is expressed in (13), where a double loop control of IC is involved.

$$\begin{cases} \Delta d_{\mathrm{d}} = G_i(G_u(\Delta u_{\mathrm{dcref}} - \Delta u_{\mathrm{dc}})) + \Delta u_{\mathrm{d}} - \omega L\Delta i_{\mathrm{q}} \\ \Delta d_{\mathrm{q}} = G_i(\Delta i_{\mathrm{qref}} - \Delta i_{\mathrm{q}}) + \Delta u_{\mathrm{q}} + \omega L\Delta i_{\mathrm{d}} \end{cases} \tag{13}$$

where $G_u = k_{pu} + k_{iu}/s$ and $G_i = k_{pi} + k_{ii}/s$ are the PI controller of the outer voltage loop and inner current loop.

3.1.3. Network model of AC/DC MG

Since each ac-DG has an independent SRF, the measurement variables should be transformed into the standard SRF for analysis [39]. The transformation of SRF follows (14).

$$\begin{bmatrix} s_{\mathrm{D}} \\ s_{\mathrm{Q}} \end{bmatrix} = \begin{bmatrix} \cos(\theta) & -\sin(\theta) \\ \sin(\theta) & \cos(\theta) \end{bmatrix} \begin{bmatrix} s_{\mathrm{d}} \\ s_{\mathrm{q}} \end{bmatrix} \tag{14}$$

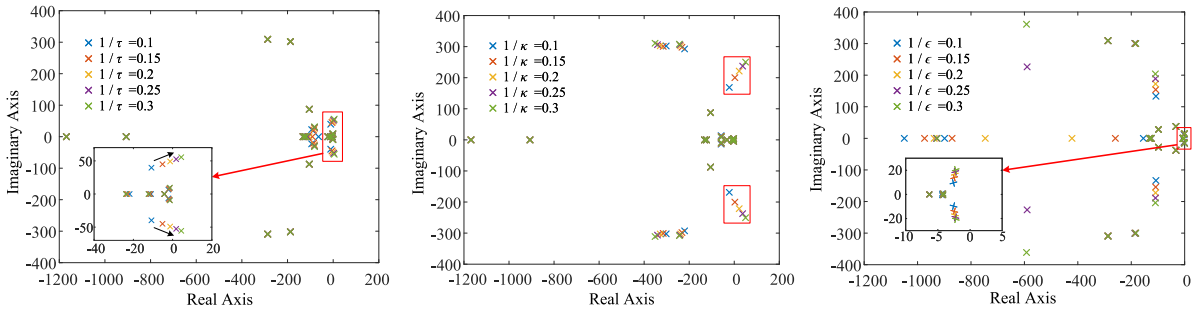

Fig. 3. Distribution of characteristic poles under variation of control parameters. (a)$1/\tau$ changes from 0.1 to 0.3. (2) $1/\kappa$ changes from 0.1 to 0.3. (c)$1/\epsilon$ changes from 0.1 to 0.3.

where s_D and s_Q are the variables of the standard SRF, and s_d and s_q are the variables with respect to their respective SRF. θ is the angle difference between the two SRFs.

Linearization is carried out in (14) at the steady-state operation point, as depicted in (15).

$$\begin{bmatrix} \Delta s_D \\ \Delta s_Q \end{bmatrix} = \begin{bmatrix} \cos(\Theta) & -\sin(\Theta) \\ \sin(\Theta) & \cos(\Theta) \end{bmatrix} \begin{bmatrix} \Delta s_d \\ \Delta s_q \end{bmatrix} + \begin{bmatrix} -\sin(\Theta) & -\cos(\Theta) \\ \cos(\Theta) & -\sin(\Theta) \end{bmatrix} \begin{bmatrix} S_d \\ S_q \end{bmatrix} \Delta\theta \tag{15}$$

where Θ is the steady state value of θ and $\Delta\theta$ is the small-signal of θ. It should be noted that the angle $\Delta\theta$ can be derived from the angular frequency $\Delta\omega$ as $\Delta\theta = \Delta\omega/s$.

Small-signal stability analysis for ac-MG is specified regarding a single bus structure. Other cases considering complicated structures can be deduced in the same way. The small-signal model of an ac-MG can be expressed by (16).

$$\begin{aligned} &\begin{bmatrix} \Delta u_{D0} \\ \Delta u_{Q0} \end{bmatrix} - \begin{bmatrix} R_0 + sL_0 & -\omega L_0 \\ \omega L_0 & R_0 + sL_0 \end{bmatrix} \begin{bmatrix} \Delta i_{D0} \\ \Delta i_{Q0} \end{bmatrix} \\ &= \begin{bmatrix} \Delta u_{D1} \\ \Delta u_{Q1} \end{bmatrix} - \begin{bmatrix} R_1 + sL_1 & -\omega L_1 \\ \omega L_1 & R_1 + sL_1 \end{bmatrix} \begin{bmatrix} \Delta i_{D1} \\ \Delta i_{Q1} \end{bmatrix} \\ &= \cdots \\ &= \begin{bmatrix} \Delta u_{D\mathcal{N}_{ac}} \\ \Delta u_{Q\mathcal{N}_{ac}} \end{bmatrix} - \begin{bmatrix} R_{\mathcal{N}_{ac}} + sL_{\mathcal{N}_{ac}} & -\omega L_{\mathcal{N}_{ac}} \\ \omega L_{\mathcal{N}_{ac}} & R_{\mathcal{N}_{ac}} + sL_{\mathcal{N}_{ac}} \end{bmatrix} \begin{bmatrix} \Delta i_{D\mathcal{N}_{ac}} \\ \Delta i_{Q\mathcal{N}_{ac}} \end{bmatrix} \\ &= \begin{bmatrix} R_{load} + sL_{load} & -\omega L_{load} \\ \omega L_{load} & R_{load} + sL_{load} \end{bmatrix} \sum_{i=0}^{\mathcal{N}_{ac}} \begin{bmatrix} \Delta i_{Di} \\ \Delta i_{Qi} \end{bmatrix} \end{aligned} \tag{16}$$

where R_i and L_i are the line resistance and inductance between the ith ac-DG and the AC bus. R_{load} and L_{load} are the load resistance and inductance connected to the AC bus.

As for a dc-MG, the small-signal model can be expressed by (17).

$$\begin{aligned} &\Delta u_{dc0} - R_{dc0}\Delta i_{dc0} \\ &= \Delta u_{dc1} - R_{dc1}\Delta i_{dc1} \\ &= \cdots \\ &= \Delta u_{dc\mathcal{N}_{dc}} - R_{dc\mathcal{N}_{dc}}\Delta i_{dc\mathcal{N}_{dc}} \\ &= R_{dcload} \sum_{j=0}^{\mathcal{N}_{dc}} \Delta i_{dcj} \end{aligned} \tag{17}$$

where R_{dcj} is the line impedance between the jth dc-DG and the DC bus. R_{dcload} is the load impedance connected to the DC bus.

A complete small-signal model of hybrid AC/DC MG can be denoted by (18) through (6)–(17).

$$y_{out} = G(s)u_{in} \tag{18}$$

where

$$u_{in} = [\Delta\boldsymbol{\omega}_{ref}, \Delta\boldsymbol{U}_{ref}, \Delta\boldsymbol{P}_{ref}, \Delta\boldsymbol{Q}_{ref}, \Delta\boldsymbol{u}_{dcref}, \Delta\boldsymbol{P}_{dcref}]^T$$
$$y_{out} = [\Delta\boldsymbol{u}_d, \Delta\boldsymbol{u}_q, \Delta\boldsymbol{i}_d, \Delta\boldsymbol{i}_q, \Delta\boldsymbol{u}_{dc}, \Delta\boldsymbol{i}_{dc}]^T$$

3.2. Small-signal stability analysis

Based on the small-signal model of a hybrid AC/DC MG, the influence of control parameters on small-signal stability can be analyzed. The effectiveness of this small-signal model is demonstrated through comparison with the simulation model built in PSCAD/EMTDC considering the MG shown in Fig. 1(a). The control parameters are listed in Table A.4 and the line impedance is depicted in Table A.5. The rated power ratio of the four DGs is set as 1:1:1:1.

There are three key parameters of the proposed control strategy, τ, κ and ϵ. Single parameter effect can be investigated according to the pole distribution. In Fig. 3(a), the poles gradually approach the imaginary axis as $1/\tau$ increasing from 0.1 to 0.3. The dominant poles have been marked with a red box. There exists a stable margin τ_s and the control system will become unstable if $\tau < \tau_s$. Fig. 3(b) illustrates the result of changing $1/\kappa$ from 0.1 to 0.3. It is evident that a stable margin κ_s also exists. In Fig. 3(c), the dominant poles influenced by ϵ move along the imaginary axis when $1/\epsilon$ changes from 0.1 to 0.3. According to the distribution of poles, the range of the parameter ϵ to ensure stability is quite large. In other words, it has little influence on the small-signal stability of the control system. Thus, the control parameters design will focus on τ and κ.

The proposed DSC is applied to a simulation model to demonstrate its small-signal stability. A traditional droop control strategy is conducted before $t = 1.5$ s and the DSC is activated afterward. Simulation results and pole distribution under different control parameters are shown in Fig. 4. Fig. 4(a) and Fig. 4(d) illustrate the results with proper control parameters. Fast power sharing in a hybrid MG can be achieved without power oscillation and the poles lie on the left-side of the complex plane. In Fig. 4(d), the location of poles influenced by τ and κ is far away from the imaginary axis. Results with smaller τ are shown in Fig. 4(b) and Fig. 4(e). With improper control parameters, power oscillation occurs. The oscillation frequency can be obtained from the pole distribution as shown in Fig. 4(e). The poles influenced by τ are marked with a red circle and the oscillation frequency is about $\omega_{o\tau} = 49.132$rad/s, which is basically consistent with the simulation results. Results obtained with smaller κ are shown in Fig. 4(c) and Fig. 4(f) and power oscillation also occurs. The poles influenced by κ are indicated by a green circle shown in Fig. 4(f) and the oscillation frequency is about $\omega_{o\tau} = 209.519$rad/s. The oscillation frequency caused by κ is higher than that caused by τ and the same conclusion can be drawn from simulation.

Small-signal analysis is helpful in designing control parameters. The stability margin of a specific parameter is determined by the poles distribution, where the minimum value guarantees all of the poles standing on the left-side of the complex plane. Thus the candidate control parameters are confined by this margin. The stability margin of parameters drawn from simulation results and theoretical small-signal analysis is listed in Table 2.

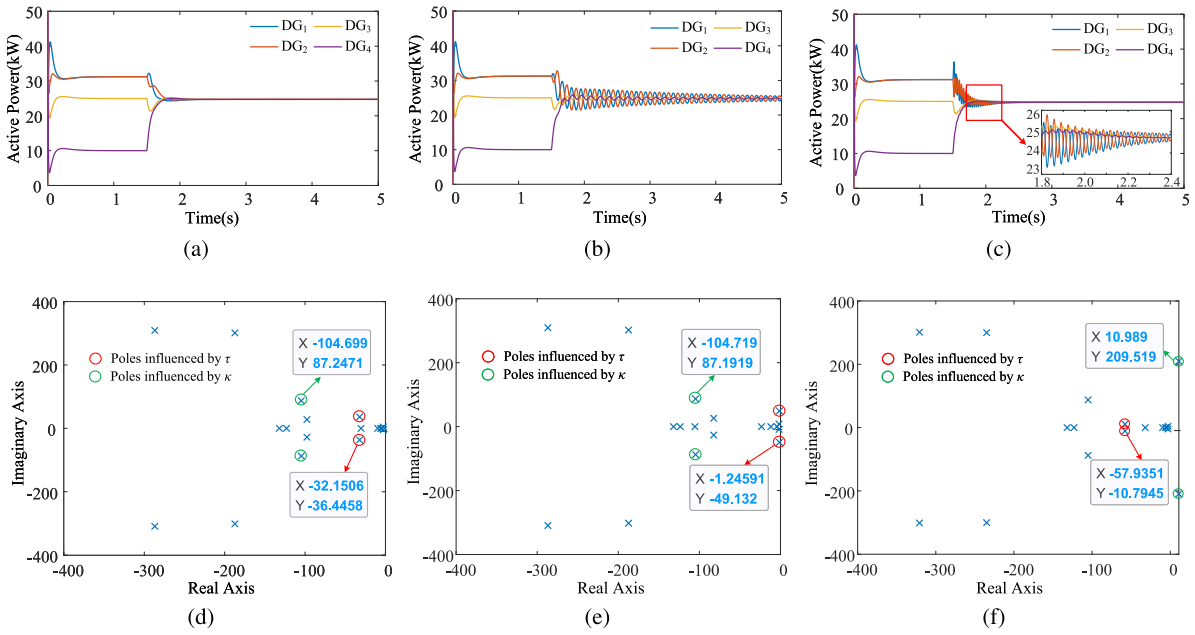

Fig. 4. Active power and pole distribution with different control parameters (DSC is put into operation at $t = 1.5$ s). (a) and (d) are resulted from the appropriate parameters ($\tau = 50, \kappa = 50, \epsilon = 50$). (b) and (e) are resulted from the parameters with a smaller τ ($\tau = 5, \kappa = 50, \epsilon = 50$). (c) and (f) are resulted from the parameters with a smaller κ ($\tau = 50, \kappa = 5.88, \epsilon = 50$).

Table 2
Stability margin corresponding to control parameters.

	Small-signal model	Simulation
$1/\tau_s$	0.21	0.23
$1/\kappa_s$	0.14	0.17

4. Experiment results

4.1. Experiment setup

In order to verify the feasibility of the proposed control strategy, a hybrid AC/DC MG experiment platform is established in the laboratory, which is shown in Fig. 5(a). The topology of this AC/DC MG is depicted in Fig. 5(b). Voltage source converter (VSC) and system parameters of the AC/DC MG are detailed in Table A.6. VSC 1 and VSC 2 are used as two ac-DGs while VSC 3 is used as a dc-DG. There are $900 + 300j$VA AC base load and 600W DC base load in the experiment. Droop control algorithm and DSC algorithm are implemented through TMS320F28335 DSP controller configured in the VSC. The controller handles measurement, control algorithm implementation, and PWM generation. The power information presented in this section is computed based on the voltage and current data measured by the DSP and transmitted via a serial port to the Raspberry Pi for storage. The Raspberry Pi is responsible for: i. Read the power information inside the controller, ii. Transmit the power information to other Raspberry Pis through wireless communication, iii. Write the power information into the DSP controller through a high-speed serial bus. All of the control parameters are listed in Table A.7.

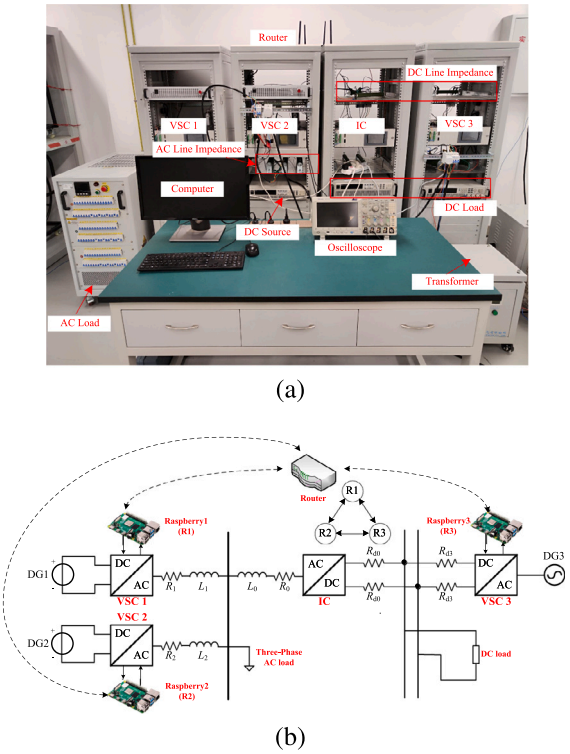

Fig. 5. Experiment platform of hybrid AC/DC MG. (a) instruments, (b) grid overview.

4.2. Control strategy verification

Herein, the proposed control strategy is verified under various operating conditions, such as AC load change, DC load change and reactive power support by IC. Power information of a VSC is measured by its DSP controller.

4.2.1. AC load change

This experiment is manipulated in three stages: i. Put the proposed control strategy into operation. ii. Increase 600 W active load in ac-MG. iii. Decrease 1200 W active load in ac-MG. The empirical results are shown in Fig. 6(a). In the first stage, the power sharing of three VSCs is realized. Fast power balance is observed when a sudden load change

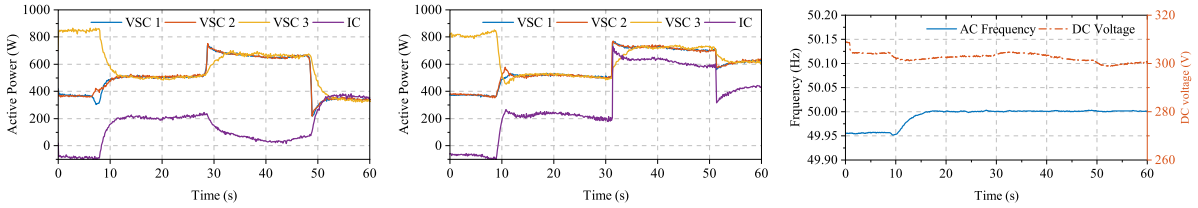

Fig. 6. Experiment results under step change of load. (a) output power under AC load change, (b) output power under DC load change, (c) AC frequency and DC voltage under DC load change.

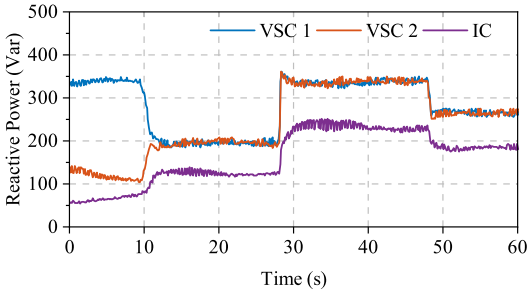

Fig. 7. Experiment results of reactive power support.

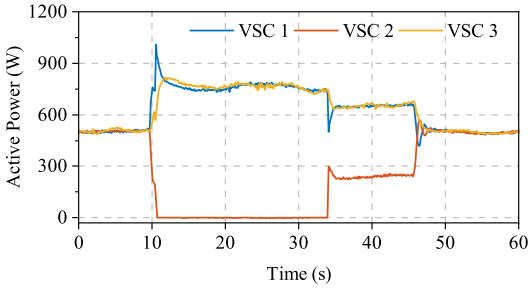

Fig. 8. Experiment results of VSC 2 plug&play.

occurs, and the IC coordinates the active power accordingly by using the local information.

4.2.2. DC load change

Following the same process, three stages are taken in a DC load change experiment: i. Put the control strategy into operation. ii. Increase 600 W active load in the dc-MG. iii. Decrease 300 W active load in the dc-MG.

From the results shown in Fig. 6(b), IC's response to DC load change is faster than its response to the AC load change, due to the fact that IC adopts a constant DC voltage control. The change of DC load will be complemented by the ac-MG through rapid power coordination of the IC. At this time, SC does not work because of its slow response. Thus the ac-DG (VSC 1 and VSC 2) responds to DC load change firstly and power sharing is realized afterwards by SC. However, the power distribution mechanism for AC load change is different. Change of AC load does not have a direct impact on dc-DG (VSC 3) before SC works. The relatively slow response of SC leads to a slow power regulation of IC when the AC load changes. Besides, AC frequency and DC voltage can be regulated within a narrow range of nominal value. As shown in Fig. 6(c), IC that does not need to communicate with DGs can regulate the DC voltage within an acceptable range of rated value. In the meantime, the AC frequency can be regulated to the nominal frequency accurately under the cooperative control of ac-DG.

4.2.3. Reactive power support of IC

In order to investigate reactive power sharing among VSCs and reactive power support of IC, the experiment is conducted through three steps: i. Put the proposed control strategy into operation. ii. Increase 600Var reactive load in the ac-MG. iii. Decrease 300Var reactive load in the ac-MG. From the results shown in Fig. 7, IC is able to support the reactive power of the ac-MG by using a $Q_{ic} - U_{ac}$ droop control.

4.3. Plug and play

Plug&play capability shows the fast quit and restart ability of the VSC when using the proposed control strategy. In this experiment, VSC 2 is offline at $t = 10$ s and restarts working at $t = 34$ s. In order to improve the synchronization stability during VSC plug&play, SC is put into operation immediately at 10 s after the VSC accessing MG. As shown in Fig. 8, DSC can work in normal operation with fast quit and restart of VSC. Power sharing can be realized among other VSCs when some of the VSCs quit. After they restart, the latter access VSCs can negotiate the power reference with the existing VSCs through the proposed DSC strategy and power sharing among all VSCs can be achieved.

4.4. Comparison under different communication network

The DSC strategy with the communication network shown in Fig. 2(b) is realized using the same experiment platform. Its performance is illustrated and compared with the communication-saving DSC strategy in this paper under two operating conditions: normal condition and IC communication failure.

4.4.1. Normal condition

The experiment follows the same process discussed in Section 4.2.1 and 4.2.2, but uses the communication network depicted in Fig. 2(b). The results are shown in Fig. 9. Power sharing is equally effective in both communication networks, but the network without IC handles the DC load variation faster and uses fewer communication links. In cases where IC communication is essential, a more extensive network of links between VSCs and IC is required, resulting in a more complex implementation process for plug&play.

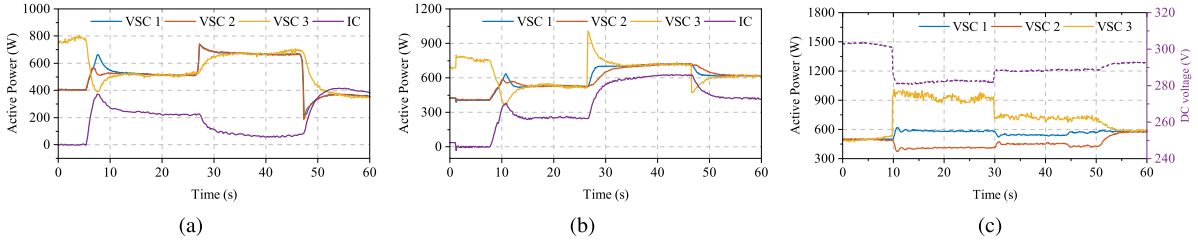

Fig. 9. Experiment results with the communication network in Fig. 2(b). (a) AC load change. (b) DC load change. (c) IC communication failure.

Table 3
Comparisons with existing DSCs.

	[32]	[34]	[36]	Proposed
Active DSC	√	√	√	√
Reactive DSC	√	√	×	√
Global power sharing	√	×	√	√
Accurate power sharing	×	√	√	√
Frequency restoration	√	√	√	√
Voltage restoration	√	√	√	×
IC communication	√	×	√	×

4.4.2. IC communication failure

Fig. 9(c) shows the active power of VSCs (solid line) and the DC bus voltage (dashed line) under IC communication failure. IC communication fails at $t = 0$ s. The DC load increases 600 W at $t = 30$ s and decreases 300 W at $t = 50$ s. IC communication recovers at $t = 50$ s. Due to a lack of communication between the IC and VSCs, the power reference of IC is hard to be adjusted by DSC. Power support in the AC/DC MG cannot be realized and an unbalanced load remains, which enforces VSCs to adjust the reference in the wrong direction and causes a larger deviation in DC voltage. Therefore, DSC is expected to quit running at this time. Fortunately, this problem can be solved if IC communication is not involved and the proposed DSC can adapt to this case.

5. Discussion

5.1. Comparison with existing DSC

Table 3 presents a comprehensive comparison between the proposed control strategy and existing DSC methods, including integrity of the control mode, control performance, and communication complexity. According to the results, the proposed approach offers a more holistic solution to DSC. It achieves an accurate AC and DC power distribution through a simple communication network, albeit with a compromise on voltage restoration. It is worth mentioning that the voltage does not deviate significantly from its rated value due to the DC voltage control and reactive power support for the IC.

In order to further evaluate the performance of different DSCs, the simulation model in Section 3.2 is utilized for a comparison with the approach presented in [32], particularly in the condition of IC communication failure. In the simulation, DSC is initiated at $t = 0.5$ s, and IC communication failure occurs at $t = 2.5$ s. At $t = 3$ s, a 20 kW load is connected to the dc-MG, and maintains without any changes afterwards. As depicted in Fig. 10, power sharing among all the DGs can be achieved after $t = 0.5$ s. However, DSC in [32] fails to achieve accurate power sharing due to the compromise between power sharing and voltage restoration. In contrast, the proposed method can maintain a high level of accuracy. It should be noted that even though the method in [32] can maintain power sharing after IC communication failure, any variation of loads may disrupt the balance. In this case, the DC voltage cannot be recovered to the rated value and poses a significant deviation. Since in the proposed method, IC communication is not required, the control performance is then not affected.

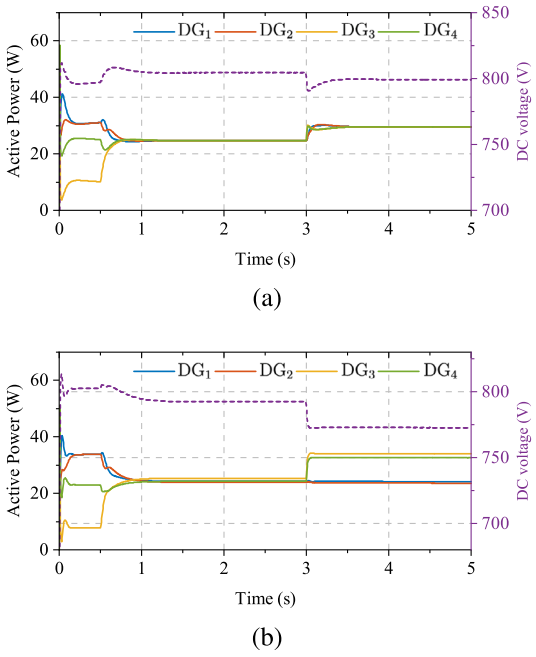

Fig. 10. Simulation results for comparison with [32]. (a) the proposed DSC. (b) DSC in [32].

5.2. Effect of communication delay

In this subsection, the effect of the communication delay is investigated by using the simulation model in Section 3.2. The results are illustrated in Fig. 11 with a delay T_d set to 0 s, 0.5 s and 1.5 s. The results indicate that minor communication delay does not impact the achievement of the control objectives, but does slow down the transient processes.

Furthermore, the influence of communication delay is integrated into the small-signal model established in (18) by introducing the delay function G_d, which can be expressed by (19) [40]. As illustrated in Fig. 12, the small-signal analysis identifies a critical communication delay of 1.8 s. If $T_d > 1.8$ s, some of the eigenvalues will enter the right half of the complex plane, posing a risk to the small-signal stability. It can be concluded that an excessive communication delay hinders the achievement of secondary control objectives.

$$G_d = e^{-sT_d} \approx \frac{1 - 0.5T_d s + 1/12T_d^2 s^2}{1 + 0.5T_d s + 1/12T_d^2 s^2} \tag{19}$$

5.3. Effect of proportional power sharing

Herein, the effectiveness of the proposed control strategy in achieving proportional power sharing is validated. Specifically, a power sharing ratio of P_{DG1}: P_{DG2}: P_{DG3}: P_{DG4} = 1:2:3:4 is implemented in the simulation model of Section 3.2. Utilizing the control Eqs. (2)–(4), the

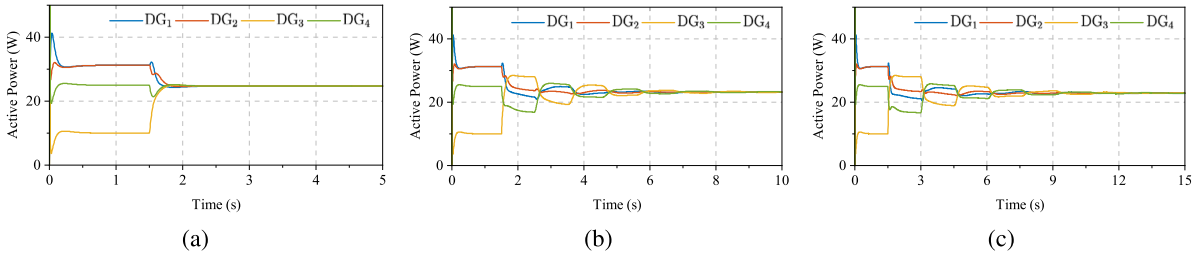

Fig. 11. Simulation results under different communication delay. (a) T_d = 0 s, (b) T_d = 0.5 s, (c) T_d = 1.5 s.

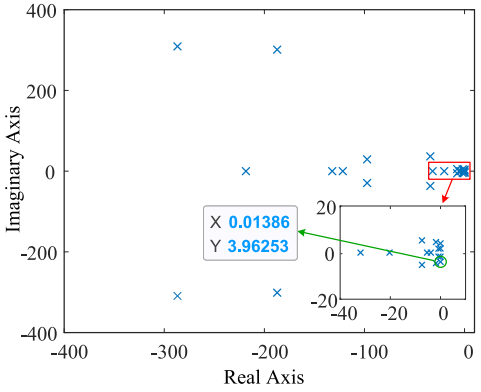

Fig. 12. Small-signal analysis with a communication delay $T_d > 1.8$ (T_d = 1.9 s).

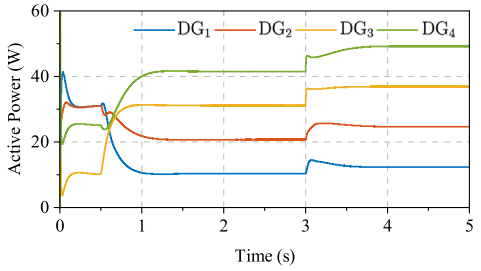

Fig. 13. Simulation results for proportional power sharing among DGs.

unit values P_i^* achieve a consensus, allowing for the adjustment of the power sharing ratio based on the rated power $S_{\text{rated}i}$. In the simulation, $S_{\text{rated}1}$: $S_{\text{rated}2}$: $S_{\text{rated}3}$: $S_{\text{rated}4}$ is set as 1:2:3:4. The simulation involves two operations: i. DSC is initiated at t = 0.5 s, ii. a 20 kW load is connected to the dc-MG at t = 3 s. The results, illustrated in Fig. 13, demonstrate that accurate proportional power sharing among DGs can be achieved.

6. Conclusion

This paper presents a novel DSC strategy for hybrid AC/DC MG. It achieves an accurate power sharing among DGs without communication links between the IC and DGs, which simplifies the overall communication network. According to the small-signal analysis, the control parameters τ and κ are crucial to small-signal stability. Instability will occur when these control parameters fall below the stability margin, specifically $\tau < \tau_s$ and $\kappa < \kappa_s$. The proposed DSC is validated on a real experimental platform under various operating conditions, including load changes and plug&play. The results demonstrate that the proposed DSC is superior to the existing methods which utilize the IC communication, particularly in the case of IC communication failure.

Table A.4
Parameters of ac-DG and dc-DG in simulation.

DG	Parameter	Value
AC	AC voltage U_{ac}	380 V
	Frequency f	50 Hz
	Active droop slope n_p	0.01 Hz/kW
	Reactive droop slope n_q	0.0002 kV/kvar
	Active power reference P_{ref}	25 kW
	Reactive power reference Q_{ref}	20 kvar
	Time constant of ASC τ	50 kW s/Hz
	Time constant of RSC κ	50 kvar s/kV
DC	DC voltage U_{dc}	800 V
	Active droop slope n_{dc}	0.002 kV/kW
	Active power reference P_{dcref}	30 kW
	Time constant of ASC ϵ	50 kW s/kV
IC	PI of voltage control k_{pu}, k_{iu}	2, 20
	PI of current control k_{pi}, k_{ii}	5, 100

CRediT authorship contribution statement

Chang Yang: Writing – review & editing, Writing – original draft, Visualization, Software, Methodology, Investigation, Formal analysis, Conceptualization. **Tao Zheng:** Writing – review & editing, Writing – original draft, Supervision, Resources, Methodology. **Ming Bu:** Writing – review & editing, Validation, Data curation. **Pengyu Li:** Visualization, Investigation.

Declaration of competing interest

The authors declare that they have no known competing financial interests or personal relationships that could have appeared to influence the work reported in this paper.

Data availability

No data was used for the research described in the article.

Acknowledgment

This work is supported by the Natural Science Foundation of Shaanxi Province (No.2024JC-YBMS-420) and National Natural Science Foundation of China (No.U23B20112).

Appendix A. Parameters in simulation and experiments

See Tables A.4 and A.7.

Table A.5
Line impedance of hybrid AC/DC MG in simulation.

ac-MG	Parameters/Ω	dc-MG	Parameters/Ω
Z_{L0}	$0.4+0.188j$	R_{L0}	0.2
Z_{L1}	$0.3+0.251j$	R_{L1}	0.05
Z_{L2}	$0.1+0.314j$	R_{L2}	0.15
Z_s	$1+1.199j$	R_s	16

Table A.6
System parameters of hybrid AC/DC MG in experiments.

	Parameters	Value
VSC	AC voltage	173 V
	Frequency	50 Hz
	DC voltage	300 V
	Filter inductance	1.2 mH
	Filter capacitor	16 uF
	Rated capacity	4.5 kVA
	Switching frequency	10 kHz
ac-MG	R_0, L_0	0.4 Ω, 0.33 mH
	R_1, L_1	1.1 Ω, 2.67 mH
	R_2, L_2	0.7 Ω, 1.45 mH
	AC load	$900+300j$ VA
dc-MG	R_{d0}	0.5 Ω
	R_{d3}	1 Ω
	DC load	600 W

Table A.7
Control parameters of hybrid AC/DC MG in experiments.

	Parameters	Value
VSC 1	Active power reference	600 W
	Reactive power reference	300 Var
	Active droop slope	0.005 Hz/kW
	Reactive droop slope	20 V/kvar
	Constant of ASC τ	10 kW s/Hz
	Constant of RSC κ	0.2 kvar s/kV
	Restoration coefficient α	1 kW/Hz
	Communication rate	50 Hz
VSC 2	Active power reference	400 W
	Reactive power reference	0 Var
	Active droop slope	0.005 Hz/kW
	Reactive droop slope	20 V/kvar
	Constant of ASC τ	10 kW s/Hz
	Constant of RSC κ	0.2 kvar s/kV
	Communication rate	50 Hz
VSC 3	Active power reference	1000 W
	Active droop slope	30 V/kW
	Constant of ASC ϵ	0.04 kW s/kV
	Communication rate	50 Hz
IC	Rated DC Voltage	300 V
	Rated AC voltage	173 V
	Coefficient of reactive support n_{ic}	0.2 A/V

References

[1] J. Choi, S.I. Habibi, A. Bidram, Distributed finite-time event-triggered frequency and voltage control of ac microgrids, IEEE Trans. Power Syst. 37 (3) (2022) 1979–1994.

[2] P. Teimourzadeh Baboli, Flexible and overall reliability analysis of hybrid ac–dc microgrid among various distributed energy resource expansion scenarios, IET Gener. Transm. Distrib. 10 (16) (2016) 3978–3984.

[3] K. Rajesh, S. Dash, R. Rajagopal, R. Sridhar, A review on control of ac microgrid, Renew. Sust. Energ. Rev. 71 (2017) 814–819.

[4] J.M. Guerrero, J.C. Vasquez, J. Matas, L.G. De Vicuna, M. Castilla, Hierarchical control of droop-controlled ac and dc microgrids—A general approach toward standardization, IEEE Trans. Ind. Electron. 58 (1) (2011) 158–172.

[5] D.E. Olivares, A. Mehrizi-Sani, A.H. Etemadi, C.A. Canizares, R. Iravani, M. Kazerani, A.H. Hajimiragha, O. Gomis-Bellmunt, M. Saeedifard, R. Palma-Behnke, G.A. Jimenez-Estevez, N.D. Hatziargyriou, Trends in microgrid control, IEEE Trans. Smart Grid 5 (4) (2014) 1905–1919.

[6] L. Ahmethodzic, M. Music, Comprehensive review of trends in microgrid control, Renew. Energy Focus 38 (2021) 84–96.

[7] S.K. Sahoo, A.K. Sinha, N.K. Kishore, Control techniques in ac, dc, and hybrid ac–dc microgrid: A review, IEEE Trans. Emerg. Sel. Topics Power Electron. 6 (2) (2018) 738–759.

[8] J.W. Simpson-Porco, Q. Shafiee, F. Dörfler, J.C. Vasquez, J.M. Guerrero, F. Bullo, Secondary frequency and voltage control of islanded microgrids via distributed averaging, IEEE Trans. Ind. Electron. 62 (11) (2015) 7025–7038.

[9] W. Gu, G. Lou, W. Tan, X. Yuan, A nonlinear state estimator-based decentralized secondary voltage control scheme for autonomous microgrids, IEEE Trans. Power Syst. 32 (6) (2017) 4794–4804.

[10] A. Milczarek, M. Malinowski, J.M. Guerrero, Reactive power management in islanded microgrid—proportional power sharing in hierarchical droop control, IEEE Trans. Smart Grid 6 (4) (2015) 1631–1638.

[11] Y. Han, P. Shen, X. Zhao, J.M. Guerrero, An enhanced power sharing scheme for voltage unbalance and harmonics compensation in an islanded ac microgrid, IEEE Trans. Energy Convers. 31 (3) (2016) 1037–1050.

[12] H. Xin, R. Zhao, L. Zhang, Z. Wang, K.P. Wong, W. Wei, A decentralized hierarchical control structure and self-optimizing control strategy for f-p type dgs in islanded microgrids, IEEE Trans. Smart Grid 7 (1) (2016) 3–5.

[13] M. Savaghebi, A. Jalilian, J.C. Vasquez, J.M. Guerrero, Secondary control scheme for voltage unbalance compensation in an islanded droop-controlled microgrid, IEEE Trans. Smart Grid 3 (2) (2012) 797–807.

[14] S. Peyghami, H. Mokhtari, P. Davari, P.C. Loh, F. Blaabjerg, On secondary control approaches for voltage regulation in dc microgrids, IEEE Trans. Ind. Appl. 53 (5) (2017) 4855–4862.

[15] A. Tah, D. Das, An enhanced droop control method for accurate load sharing and voltage improvement of isolated and interconnected dc microgrids, IEEE Trans. Sustain. Energy 7 (3) (2016) 1194–1204.

[16] Y. Li, Z. Zhang, T. Dragicevic, J. Rodriguez, A unified distributed cooperative control of dc microgrids using consensus protocol, IEEE Trans. Smart Grid 12 (3) (2021) 1880–1892.

[17] V. Nasirian, S. Moayedi, A. Davoudi, F.L. Lewis, Distributed cooperative control of dc microgrids, IEEE Trans. Power Electron. 30 (4) (2015) 2288–2303.

[18] M. Yuan, Y. Fu, Y. Mi, Z. Li, C. Wang, Hierarchical control of dc microgrid with dynamical load power sharing, Appl. Energy 239 (2019) 1–11.

[19] A.A. Hamad, M.A. Azzouz, E.F. El-Saadany, Multiagent supervisory control for power management in dc microgrids, IEEE Trans. Smart Grid 7 (2) (2016) 1057–1068.

[20] X. Liu, P. Wang, P.C. Loh, A hybrid ac/dc microgrid and its coordination control, IEEE Trans. Smart Grid 2 (2) (2011) 278–286.

[21] X. Lu, J.M. Guerrero, K. Sun, J.C. Vasquez, R. Teodorescu, L. Huang, Hierarchical control of parallel ac-dc converter interfaces for hybrid microgrids, IEEE Trans. Smart Grid 5 (2) (2014) 683–692.

[22] M. Hosseinzadeh, F.R. Salmasi, Power management of an isolated hybrid ac/dc micro-grid with fuzzy control of battery banks, IET Renew. Power Gener. 9 (5) (2015) 484–493.

[23] N. Eghtedarpour, E. Farjah, Power control and management in a hybrid ac/dc microgrid, IEEE Trans. Smart Grid 5 (3) (2014) 1494–1505.

[24] H. Zhang, J. Zhou, Q. Sun, J.M. Guerrero, D. Ma, Data-driven control for interlinked ac/dc microgrids via model-free adaptive control and dual-droop control, IEEE Trans. Smart Grid 8 (2) (2017) 557–571.

[25] Y. Xia, W. Wei, M. Yu, X. Wang, Y. Peng, Power management for a hybrid ac/dc microgrid with multiple subgrids, IEEE Trans. Power Electron. 33 (4) (2018) 3520–3533.

[26] P. Yang, Y. Xia, M. Yu, W. Wei, Y. Peng, A decentralized coordination control method for parallel bidirectional power converters in a hybrid ac–dc microgrid, IEEE Trans. Ind. Electron. 65 (8) (2018) 6217–6228.

[27] H.H. Huang, C.Y. Hsieh, J.Y. Liao, K.H. Chen, Adaptive droop resistance technique for adaptive voltage positioning in boost dc–dc converters, IEEE Trans. Power Electron. 26 (7) (2011) 1920–1932.

[28] W. Yao, Y. Wang, Y. Xu, C. Deng, Q. Wu, Distributed weight-average-prediction control and stability analysis for an islanded microgrid with communication time delay, IEEE Trans. Power Syst. 37 (1) (2022) 330–342.

[29] R. Zhang, B. Hredzak, Nonlinear sliding mode and distributed control of battery energy storage and photovoltaic systems in ac microgrids with communication delays, IEEE Trans. Ind. Informat. 15 (9) (2019) 5149–5160.

[30] Y. Khayat, Q. Shafiee, R. Heydari, M. Naderi, T. Dragičević, J.W. Simpson-Porco, F. Dörfler, M. Fathi, F. Blaabjerg, J.M. Guerrero, H. Bevrani, On the secondary control architectures of ac microgrids: An overview, IEEE Trans. Power Electron. 35 (6) (2020) 6482–6500.

[31] F. Gao, R. Kang, J. Cao, T. Yang, Primary and secondary control in dc microgrids: A review, J. Mod. Power Syst. Clean Energy 7 (2) (2019) 227–242.

[32] E. Espina, R. Cárdenas-Dobson, J.W. Simpson-Porco, D. Sáez, M. Kazerani, A consensus-based secondary control strategy for hybrid ac/dc microgrids with experimental validation, IEEE Trans. Power Electron. 36 (5) (2021) 5971–5984.

[33] Z. Li, Z. Cheng, J. Si, S. Li, Distributed event-triggered hierarchical control to improve economic operation of hybrid ac/dc microgrids, IEEE Trans. Power Syst. 37 (5) (2022) 3653–3668.
[34] H. Yoo, T. Nguyen, H. Kim, Consensus-based distributed coordination control of hybrid ac/dc microgrids, IEEE Trans. Sustain. Energy 11 (2) (2020) 629–639.
[35] J.J. Wang, C.Y. Dong, C. Jin, P.F. Lin, P. Wang, Distributed uniform control for parallel bidirectional interlinking converters for resilient operation of hybrid ac/dc microgrid, IEEE Trans. Sustain. Energy 13 (1) (2022) 3–13.
[36] J.D. Watson, I. Lestas, Frequency and voltage regulation in hybrid ac/dc networks, IEEE Trans. Control Syst. Technol. 29 (5) (2021) 1839–1849.
[37] F. Nejabatkhah, Y.W. Li, Overview of power management strategies of hybrid ac/dc microgrid, IEEE Trans. Power Electron. 30 (12) (2015) 7072–7089.
[38] W. Rui, S. Qiuye, Z. Pinjia, G. Yonghao, Q. Dehao, W. Peng, Reduced-order transfer function model of the droop-controlled inverter via jordan continued-fraction expansion, IEEE Trans. Energy Convers. 35 (3) (2020) 1585–1595.
[39] S. Wang, Z. Liu, J. Liu, D. Boroyevich, R. Burgos, Small-signal modeling and stability prediction of parallel droop-controlled inverters based on terminal characteristics of individual inverters, IEEE Trans. Power Electron. 35 (1) (2020) 1045–1063.
[40] Y. Li, Z. Shuai, J. Fang, X. Wu, Z.J. Shen, Small-signal stability analysis method for hybrid ac–dc systems with multiple dc buses, IEEE Trans. Emerg. Sel. Topics Circuits Syst. 11 (1) (2020) 17–27.